Simulation of Sample Inhomogeneity in Microwave Impedance Microscopy

Timothy S. Jones*[1], Carlos R. Pérez[2], and Jorge J. Santiago-Avilés[1]
[1]Department of Electrical and Systems Engineering, University of Pennsylvania, [2]Department of Materials Science and Engineering, University of Pennsylvania
*Corresponding author: 200 S 33rd Street, Room 203 Moore Building, Philadelphia, PA 19104, jonests@seas.upenn.edu

Abstract: Microwave impedance microscopy (MIM) is a novel mode of near-field scanning probe microscopy that can measure topography and local electrical impedance simultaneously with nanometer spatial resolution. MIM is often used qualitatively to identify defects in nanodevices or to image ferroelectric domain walls, for example. We have chosen to use MIM to study the disordered pore networks of nanostructured carbon materials, such as carbide-derived carbon (CDC) and onion-like carbon (OLC). In this work, we model MIM experiments by simulating the electrical response of some simple models of heterogeneous materials under an AFM tip which radiates an RF electromagnetic field. These models are designed to act as very basic approximations of more complicated structures measured with the MIM technique, with the eventual goal of correlating the electrical response with local structural parameters, such as porosity.

Keywords: microwave impedance microscopy, near-field scanning microwave microscopy, inhomogeneity

1. Introduction

The recent proliferation of scanning probe microscopy techniques that interrogate electromagnetic phenomena in the near-field is predated by an article by E.H. Synge in 1928 [1] which proposes the use of a small colloidal particle to scatter incident radiation toward a sample held in very close proximity. The portion of radiation transmitted was to be collected through an objective lens as the optical probe was scanned over the sample. The realization of this technique had to wait several decades, with a functioning optical microscope not produced until 1984 [2], mainly enabled by the invention of the scanning tunneling microscope.

Today, near-field microscopes abound. Increasingly capable atomic force microscope chassis offer a very convenient means of coupling highly localized electromagnetic radiation to a sample. The access to local material properties that such instruments provide promises to produce great advances across chemistry, physics, and materials science [3,4].

2. Materials

While well-ordered, crystalline materials have a mature theoretical framework for structural analysis, inhomogeneous and disordered systems are often more difficult to characterize. Biological materials, porous solids, dispersions, and other relatively amorphous systems are all subjects of great attention in materials research and, due to their heterogeneous and varied micro and nanostructures, all stand to benefit from access to local properties by functional scanning probes. We have chosen to study different nanostructured carbon materials with local probes because of the diverse and often controllable morphology of these materials, as well as their varied applications in energy storage, medicine, tribology, and other settings. A description of two examples of these materials is given below.

2.1 Carbide-derived Carbon

Carbide-derived carbon (CDC) can refer to a large group of both ordered and disordered structures, but here the discussion is restricted to relatively amorphous, porous carbon, chosen here for its structural tunability and consequently its expected ability to exhibit some diversity when investigating the relationship between morphology and electrical response. In the synthesis of this type of CDC, a carbide precursor, of which a variety of well-studied binary and ternary compounds exist, is subjected to one of a few chemical or physical processes known to extract the metal atoms from their bonded carbons [5]. Among the most common synthesis methods is a heat treatment in a chlorine environment. After the metal atoms are removed, a disordered network of porous carbon remains. Through the

choice of precursor, control of the temperature and the halogen to carbon ratio in the synthesis reaction, and control of conditions in a post-synthesis cleaning and annealing step, one can rather precisely influence the nanoscale structure of that network. The features that may be tuned include the specific surface area, porosity (the volumetric complement of the carbon), the pore size distribution, and the degree of structural order in the carbon itself. The high bulk porosity > 50% by volume) and high specific surface area (>2000 m^2/g especially the tunability of CDC make this material attractive in many applications, including electrochemical capacitors, fuel cell catalyst support, tribological coatings, and biofluid purification [5].

2.2 Onion-like Carbon

Onion-like carbon (OLC) is a graphitic, multi-shell fullerene-like particle. OLC can be found along with amorphous CDC in the carbon products yielded from carbide halogenation, but is most commonly and conveniently synthesized by the vacuum annealing of nanoscopic diamond particles [6,7]. The nanodiamonds themselves are found in the carbonaceous soot left by the detonation of high explosives. In annealing the nanodiamond at temperatures above 1200ºC, the sp^3-bonded content is transformed into closed and layered sp^2 shells, while lower temperatures or incomplete annealing may preserve the diamond core within the shells to some degree. The 5 to 10 nm particles are mostly defect-free, giving rise to a high electrical conductivity. As such, and despite the fact that OLC agglomerates have no internal porosity like CDC, OLC has been shown to perform favorably as electrodes for electrochemical capacitors [7], as well as a conductive additives for other materials.

3. Methods

Microwave impedance microscopy [8] is a recently developed mode of AFM that has been commercialized as the scanning MIM (sMIM) mode by PrimeNano and Asylum Research. The instrument is not the first of its kind [9,10] but represents the advancement of such instruments out of the academic environment. Keysight Technologies (formerly of Agilent Technologies) also markets a similar commercial AFM mode called scanning microwave microscopy (SMM).

Of the variety of scanning near-field microscopes in literature, each instrument is unique in its choice of excitation and detection system, probe design, and manner of integration. The sMIM mode uses cantilevers that are shielded up to the tip to provide very low stray capacitance and series resistance [11]. The SMM mode is representative of instruments that use broadband electronics—SMM itself utilizes a vector network analyzer—to excite fields at the probe and measure the response, whereas sMIM and others use a resonator circuit at a fixed frequency (3 GHz in this case) as the microwave source. sMIM also uses an impedance matching element placed between the probe and the source and detection electronics to maximize the power transferred to the tip and optimize the measurement sensitivity. The change in the impedance of the sample, as manifested by variation in the reflected signal, is reported as its real and imaginary parts as the probe scans over the surface point by point. Topography is measured simultaneously by the usual AFM facilities, so the result of a measurement is overlapping maps of topography and changes in resistance and reactance of the tip-sample system.

4. Use of COMSOL Multiphysics

Because the size of the sample is much smaller than the 3 GHz free space wavelength (10 cm), it is assumed that MIM measures interactions with near-field, evanescent waves only. We can therefore use a quasistatic approximation of Maxwell's equations, implemented by COMSOL Multiphysics for finite element analysis in the Electric Currents interface of the AC/DC module. For a frequency domain study, COMSOL solves a current conservation equation based on Ohm's law along with a term for displacement current

$$\mathbf{J} = \sigma\mathbf{E} + j\omega\mathbf{D}$$

From these results, COMSOL also readily computes the admittance between terminals, giving an output similar to an actual MIM measurement.

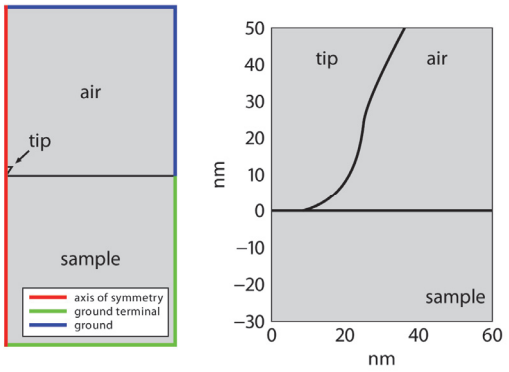

Figure 1. The geometry of a 2D axisymmetric simulation corresponding to the tip-sample system in a MIM experiment. A signal is applied to the top plane of a conical tip and the admittance is measured between the tip and the outer edges of the sample region.

We use a 2D axisymmetric model to exploit the rotational symmetry in a first approximation of the tip-sample system—tips are actually pyramidal. The geometry of the simulation is shown in Figure 1 along with a magnified view of the tip-sample contact. The cylindrical geometry has a radius of 500 μm; this distance was chosen so that the impedance between the tip and sample settled to a near-constant value within several orders of magnitude. Also note that in the figure, two ground nodes are shown, one "ground terminal," and the other simply "ground." Both are held at zero volts, however it is only the current summed between the source (the top plane of the conical tip) and the edges of the sample (the "ground terminal") that contributes to the calculated changes in admittance.

5. Results & Discussion

For the case of the homogeneous samples (Figure 1), as the sample conductivity is swept between 10^{-4} and 10^{4} S/m, changes in the real and imaginary parts of the tip-sample system are observed. The response curves, along with an equivalent circuit with which they are in very close agreement, are shown in Figure 2. The interpretation of the response curves in light of the equivalent circuit is simple. The real part of the admittance is dominated by the G_1 parameter and simply changes linearly with respect to conductance, as in Ohm's law. The behavior of the imaginary part stems from the right-hand branch of the model. In the high conductivity range, G_2 is very large and shorts C_2, leaving C_1 to determine the response. In the low conductivity limit, G_2 is very small and the circuit branch reduces to a series combination of two capacitors, of capacitance necessarily smaller than C_1 alone. The toggling between these two extremes gives rise to the two levels of the imaginary response curve.

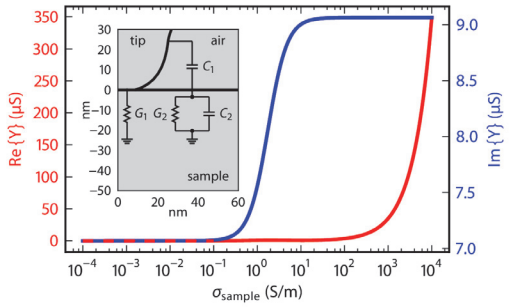

Figure 2. The real and imaginary parts of the simulated admittance between the tip and a homogeneous sample, swept in conductivity. The response is easily fitted to an equivalent circuit, pictured.

In the equivalent circuit, it can be assumed that both G_1 and G_2 are directly dependent on the sample conductivity, that is that $G_1=k_1\sigma$ and $G_2=k_2\sigma$. By dimensional analysis, k_1 and k_2 must have units of meters. The same result can be found and an estimation of k_1 or k_2 based on sample geometry by considering that the equipotential lines in the sample are approximately circular, suggesting an easily computable integral for the total conductance as that of a hemispherical conductor. This model has been suggested previously [12]. In the simulations in this work, we consider k_1 as a possible indicator of the real part of the tip-sample impedance as it is affected by different pore spaces, regardless of the base conductivity of the host material.

In order to determine the size of the volume interrogated by the probe, a single inclusion was placed at various points in a grid underneath the tip. In Figure 3, a map of the normalized k_1 parameter is shown. From the figure it is evident that only inclusions placed within 20 to 30 nm away from the contact will result in a significant change in tip-sample admittance. Outside of this region, isolated inclusions will appear indistinguishable from a homogeneous sample.

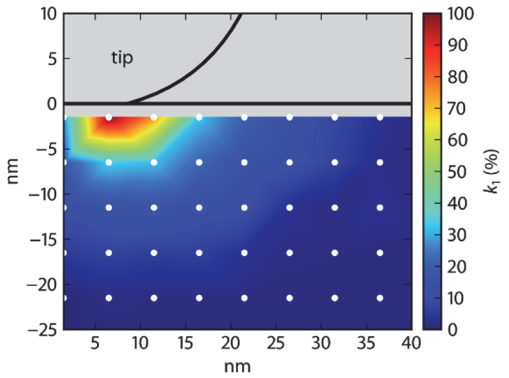

Figure 3. The normalized k_1 parameter for a non-conducting inclusion placed at various positions in an otherwise homogeneous sample. The quick decay away from the tip-sample contact indicates the region of sensitivity.

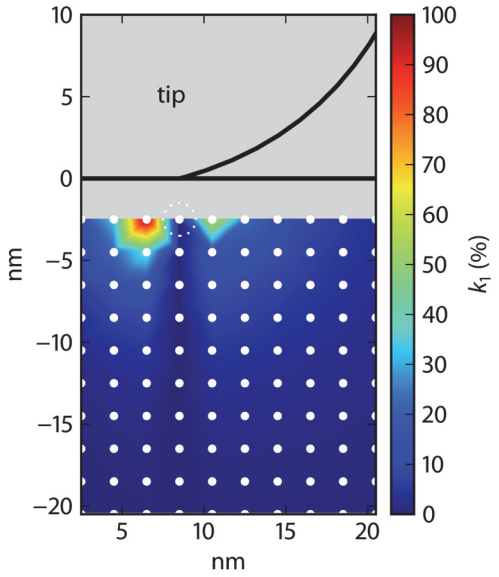

Figure 4. The normalized k_1 parameter for a non-conducting inclusion placed at a fixed position below the tip, with another inclusion placed at various positions on a grid. The results indicate the effects of one inclusion on the visibility of others.

At intermediate and high conductivities, most of the real part tip-sample admittance is due to the parameter G_1. As the tip contact area represents the narrowest cross-section for current flow between the tip terminal and the ground at the edges of the sample, it represents the region most sensitive to additional resistive inclusions. This can be seen by the results shown in Figure 4, where a single inclusion was held fixed near the tip-sample contact, and an additional inclusion was placed at different positions in the volume below.

6. Future Work

The sMIM instrument has not yet been rigorously characterized. Questions may arise as to how much the sample is affected by the mechanical stress the tip or even perhaps the microwave power imparted by the tip. Likewise, the assumption that only evanescent fields are excited in the sample has not been explicitly validated. Further simulations may help to address some of these concerns.

Also, in the effort to build a correspondence between the measurements of heterogeneous, nanostructured materials and their electromagnetic response with the aid of FEM simulations, it will be helpful to validate this model with real measurements of more simply structured samples. Simple samples, such as dielectric spheres in a carbon matrix of low porosity, will be prepared that more closely approximate the simplest analytical and numerical models. Experiments are planned for samples with silica and polystyrene nanospheres embedded in an activated carbon host with varying amounts of a PTFE binder. The spherical inclusions are more easily mimicked in FEM simulations and offer a more simple geometry for modelling and analysis, thereby facilitating the validation of more complex models of real MIM measurements on the tortuous pore networks present in the CDC and OLC materials already discussed.

7. Conclusions

This work attempts some beginning steps toward clarifying an understanding of how local electric fields applied by nanoscopic probes interact with heterogeneous materials. Non-conducting inclusions were placed in a sample of varying conductivity in different configurations to test if the reflected signal is affected.

8. References

1. E. H. Synge, A Suggested Method for Extending Microscopy Resolution into the Ultra-

Microscope Region, *Philosophical Magazine*, **6**, 356–362 (1928)
2. D. W. Pohl, W. Denk, and M. Lanz, Optical Stethoscopy: Image Recording with Resolution λ/20, *Applied Physics Letters*, **44**, 651–653 (1984)
3. Dawn Bonnell, Pushing Resolution Limits of Functional Imaging to Probe Atomic Scale Properties, *ACS Nano*, **2**, 1753–1759 (2008)
4. Dawn Bonnell et al., Imaging Physical Phenomena with Local Probes: From Electrons to Photons, *Reviews of Modern Physics*, **84**, 1343–1381 (2012)
5. V. Presser, M. Heon, and Y. Gogotsi, Carbide-Derived Carbons – From Porous Networks to Nanotubes and Graphene, *Advanced Functional Materials*, **21**, 810–833 (2011)
6. V. L. Kuznetsov et al., Effect of Explosion Conditions on the Structure of Detonation Soots: Ultradisperse Diamond and Onion Carbon, *Carbon*, **32**, 873–882 (1994)
7. J. K. McDonough et al., Influence of the Structure of Carbon Onions on Their Electrochemical Performance in Supercapacitor Electrodes, *Carbon*, **50**, 3298–3309 (2012)
8. K. Lai et al., Atomic-force-microscope-compatible Near-field Scanning Microwave Microscope with Separated Excitation and Sensing Probes, *Review of Scientific Instruments*, **78**, 063702 (2007)
9. S. Kalinin and A. Gruverman, *Scanning Probe Microscopy: Electrical and Electromechanical Phenomena at the Nanoscale*, vol. 1, 215–253. Springer, New York (2006)
10. B. T. Rosner and D. W. van der Weide, High-Frequency Near-Field Microscopy, *Review of Scientific Instruments*, **73**, 2505–2525 (2002)
11. Y. Yang et al., Batch-fabricated Cantilever Probes with Electrical Shielding for Nanoscale Dielectric and Conductivity Imaging, *Journal of Micromechanics and Microengineering*, **22**, 115040 (2012)
12. Z. Wang et al., Quantitative Measurement of Sheet Resistance by Evanescent Microwave Probe, *Applied Physics Letters*, **86**, 153118 (2005)

9. Acknowledgements

The authors would like to thank Boris Dyatkin and Dr. Yury Gogotsi of Drexel University and Dr. Jake McDonough for providing carbon samples that act as the motivation of this work. We also thank Asylum Research and PrimeNano for sharing time on an sMIM instrument. This work was partially supported by the Department of Energy Office of Basic Science grant DE-FG02-00ER45813-A000, and the Nano/Bio Interface Center of the University of Pennsylvania, via the National Science Foundation NSEC DMR08-32802 fund.